IV

Time Meets Frequency

When we listen to music, we clearly "hear" the time variation of the sound "frequencies." These localized frequency events are not pure tones but packets of close frequencies. The properties of sounds are revealed by transforms that decompose signals over elementary functions that are well concentrated in time and frequency. Windowed Fourier transforms and wavelet transforms are two important classes of local time-frequency decompositions. Measuring the time variations of "instantaneous" frequencies illustrates the limitations imposed by the Heisenberg uncertainty. These instantaneous frequencies are detected as local maxima in windowed Fourier and wavelet dictionaries, and define a signal approximation support. Audio processing algorithms are implemented by modifying the geometry of this approximation support.

There is no unique definition of time-frequency energy density. All quadratic time-frequency distributions are related through the averaging of a single quadratic form called the Wigner-Ville distribution. This framework gives another perspective on windowed Fourier and wavelet transforms.

4.1 Time-Frequency Atoms

A linear time-frequency transform correlates the signal with a dictionary of waveforms that are well concentrated in time and in frequency. These waveforms are called *time-frequency atoms*. Let us consider a general dictionary of time-frequency atoms $\mathcal{D} = \{\phi_\gamma\}_{\gamma\in\Gamma}$, where γ might be a multi-index parameter. We suppose that $\phi_\gamma \in \mathbf{L^2}(\mathbb{R})$ and that $\|\phi_\gamma\| = 1$. The corresponding linear time-frequency transform of $f \in \mathbf{L^2}(\mathbb{R})$ is defined by

$$\Phi f(\gamma) = \int_{-\infty}^{+\infty} f(t)\, \phi_\gamma^*(t)\, dt = \langle f, \phi_\gamma \rangle.$$

The Parseval formula (2.25) proves that

$$\Phi f(\gamma) = \int_{-\infty}^{+\infty} f(t)\, \phi_\gamma^*(t)\, dt = \frac{1}{2\pi} \int_{-\infty}^{+\infty} \hat{f}(\omega)\, \hat{\phi}_\gamma^*(\omega)\, d\omega. \tag{4.1}$$

If $\phi_\gamma(t)$ is nearly zero when t is outside a neighborhood of an abscissa u, then $\langle f, \phi_\gamma \rangle$ depends only on the values of f in this neighborhood. Similarly, if $\hat{\phi}_\gamma(\omega)$ is negligible for ω far from ξ, then the

right integral of (4.1) proves that $\langle f, \phi_\gamma \rangle$ reveals the properties of $\hat{f}$ in the neighborhood of ξ.

Heisenberg Boxes The slice of information provided by $\langle f, \phi_\gamma \rangle$ is represented in a time-frequency plane (t, ω) by a region whose location and width depends on the time-frequency spread of ϕ_γ. Since

$$\|\phi_\gamma\|^2 = \int_{-\infty}^{+\infty} |\phi_\gamma(t)|^2 \, dt = 1,$$

we interpret $|\phi_\gamma(t)|^2$ as a probability distribution centered at

$$u_\gamma = \int_{-\infty}^{+\infty} t \, |\phi_\gamma(t)|^2 \, dt. \tag{4.2}$$

The spread around u_γ is measured by the variance

$$\sigma_t^2(\gamma) = \int_{-\infty}^{+\infty} (t - u_\gamma)^2 \, |\phi_\gamma(t)|^2 \, dt. \tag{4.3}$$

The Plancherel formula (2.26) proves that $\int_{-\infty}^{+\infty} |\hat{\phi}_\gamma(\omega)|^2 \, d\omega = 2\pi \|\phi_\gamma\|^2$. The center frequency of $\hat{\phi}_\gamma$ is therefore defined by

$$\xi_\gamma = \frac{1}{2\pi} \int_{-\infty}^{+\infty} \omega \, |\hat{\phi}_\gamma(\omega)|^2 \, d\omega, \tag{4.4}$$

and its spread around ξ_γ is

$$\sigma_\omega^2(\gamma) = \frac{1}{2\pi} \int_{-\infty}^{+\infty} (\omega - \xi_\gamma)^2 \, |\hat{\phi}_\gamma(\omega)|^2 \, d\omega. \tag{4.5}$$

The time-frequency resolution of ϕ_γ is represented in the time-frequency plane (t, ω) by a Heisenberg box centered at (u_γ, ξ_γ), whose width along time is $\sigma_t(\gamma)$ and whose width along frequency is $\sigma_\omega(\gamma)$. This is illustrated by Figure 4.1. The Heisenberg uncertainty Theorem 2.6 proves that the area of the rectangle is at least $1/2$:

$$\sigma_t \, \sigma_\omega \geqslant \frac{1}{2}. \tag{4.6}$$

This limits the joint resolution of ϕ_γ in time and frequency. The time-frequency plane must be manipulated carefully because a point (t_0, ω_0) is ill-defined. There is no function that is perfectly well concentrated at a point t_0 and a frequency ω_0. Only rectangles with area at least $1/2$ may correspond to time-frequency atoms.

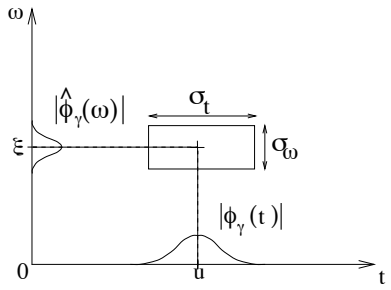

Figure 4.1: Heisenberg box representing an atom ϕ_γ.

Translation Invariant Dictionaries For pattern recognition, it can be important to construct signal representations that are translation invariant. When a pattern is translated, its numerical descriptors are then translated but not modified. Observe that for any $\phi_\gamma \in \mathcal{D}$ and any shift u

$$\langle f(t-u), \phi_\gamma(t)\rangle = \langle f(t), \phi_\gamma(t+u)\rangle \ .$$

A translation invariant representation is thus obtained if $\phi_\gamma(t+u)$ is in $\mathcal{D}$ up to a multiplicative constant. Such a dictionary is said to be translation invariant.

A translation invariant dictionary is obtained by translating a family of generators $\{\phi_\gamma\}_{\gamma\in\Gamma}$, and can be written $\mathcal{D} = \{\phi_{u,\gamma}\}_{\gamma\in\Gamma, u\in\mathbb{R}}$, with $\phi_{u,\gamma}(t) = \lambda_{u,\gamma}\,\phi_\gamma(t-u)$. The resulting time-frequency transform of f can then be written as a convolution:

$$\Phi f(u,\gamma) = \langle f, \phi_{u,\gamma}\rangle = \int_{-\infty}^{+\infty} f(t)\,\lambda_{u,\gamma}\phi^*_\gamma(t-u)\,dt = \lambda_{u,\gamma}\, f \star \tilde{\phi}_\gamma(u)$$

with $\tilde{\phi}_\gamma(t) = \phi^*_\gamma(-t)$.

Energy Density Let us suppose that $\phi_\gamma(t)$ is centered at $t=0$ so that $\phi_{u,\gamma}(t)$ is centered at u. Let ξ_γ be the center frequency of $\hat{\phi}_\gamma(\omega)$ defined in (4.4). The time-frequency box of $\phi_{u,\gamma}$ specifies a neighborhood of (u,ξ_γ) where the energy of f is measured by

$$P_\Phi f(u,\xi_\gamma) = |\langle f, \phi_{u,\gamma}\rangle|^2 = \left|\int_{-\infty}^{+\infty} f(t)\,\phi^*_{u,\gamma}(t)\,dt\right|^2 . \tag{4.7}$$

Section 4.5.1 proves that any such energy density is an averaging of the Wigner-Ville distribution, with a kernel that depends on the atoms $\phi_{u,\gamma}$.

Example 4.1. *A windowed Fourier atom is constructed with a window g modulated by the frequency ξ and translated by u:*

$$\phi_{u,\gamma}(t) = g_{u,\xi}(t) = \mathrm{e}^{i\xi t}\, g(t-u). \tag{4.8}$$

The resulting window Fourier dictionary $\mathcal{D} = \{g_{u,\xi}(t)\}_{u,\xi\in\mathbb{R}^2}$ is translation invariant since $g_{u,\xi} = \mathrm{e}^{i\xi u}\, g_{0,\xi}(t-u)$. A windowed Fourier dictionary is also frequency shit invariant because

$$\mathrm{e}^{i\omega t}\, g_{u,\xi}(t) = g_{u,\xi+\omega}(t) \in \mathcal{D} \ .$$

This dictionary is thus particularly useful to analyze patterns that are translated in time and frequency.

A wavelet atom is a dilation by s and a translation by u of a mother wavelet ψ:

$$\phi_{u,\gamma}(t) = \psi_{u,s}(t) = \frac{1}{\sqrt{s}}\,\psi\left(\frac{t-u}{s}\right). \tag{4.9}$$

A wavelet dictionary $\mathcal{D} = \{\psi_{u,s}(t)\}_{u\in\mathbb{R}, s\in\mathbb{R}^+}$ translation invariant but also scale invariant, because scaling any wavelet produces a dilated wavelet that remains in the dictionary. A wavelet dictionary is well adapted to analyze patterns that are translated and scaled by arbitrary factors.

Wavelets and windowed Fourier atoms have their energy well localized in time, while their Fourier transform is mostly concentrated in a limited frequency band. The properties of the resulting transforms are studied in Sections 4.2 and 4.3.

4.2 Windowed Fourier Transform

In 1946, Gabor [266] introduced windowed Fourier atoms to measure the "frequency variations" of sounds. A real and symmetric window $g(t) = g(-t)$ is translated by u and modulated by the frequency ξ:

$$g_{u,\xi}(t) = \mathrm{e}^{i\xi t} g(t-u). \tag{4.10}$$

It is normalized $\|g\| = 1$ so that $\|g_{u,\xi}\| = 1$ for any $(u,\xi) \in \mathbb{R}^2$. The resulting windowed Fourier transform of $f \in \mathbf{L^2}(\mathbb{R})$ is

$$Sf(u,\xi) = \langle f, g_{u,\xi} \rangle = \int_{-\infty}^{+\infty} f(t)\, g(t-u)\, \mathrm{e}^{-i\xi t}\, dt. \tag{4.11}$$

This transform is also called the *short time Fourier transform* because the multiplication by $g(t-u)$ localizes the Fourier integral in the neighborhood of $t = u$.

As in (4.7), one can define an energy density called a *spectrogram*, denoted P_S:

$$P_S f(u,\xi) = |Sf(u,\xi)|^2 = \left| \int_{-\infty}^{+\infty} f(t)\, g(t-u)\, \mathrm{e}^{-i\xi t}\, dt \right|^2. \tag{4.12}$$

The spectrogram measures the energy of f in a time-frequency neighborhood of (u,ξ) specified by the Heisenberg box of $g_{u,\xi}$.

Heisenberg Boxes Since g is even, $g_{u,\xi}(t) = \mathrm{e}^{i\xi t} g(t-u)$ is centered at u. The time spread around u is independent of u and ξ:

$$\sigma_t^2 = \int_{-\infty}^{+\infty} (t-u)^2\, |g_{u,\xi}(t)|^2\, dt = \int_{-\infty}^{+\infty} t^2\, |g(t)|^2\, dt. \tag{4.13}$$

The Fourier transform $\hat{g}$ of g is real and symmetric because g is real and symmetric. The Fourier transform of $g_{u,\xi}$ is

$$\hat{g}_{u,\xi}(\omega) = \hat{g}(\omega - \xi)\, \exp[-iu(\omega - \xi)]\,. \tag{4.14}$$

It is a translation by ξ of the frequency window $\hat{g}$, so its center frequency is ξ. The frequency spread around ξ is

$$\sigma_\omega^2 = \frac{1}{2\pi} \int_{-\infty}^{+\infty} (\omega - \xi)^2\, |\hat{g}_{u,\xi}(\omega)|^2\, d\omega = \frac{1}{2\pi} \int_{-\infty}^{+\infty} \omega^2\, |\hat{g}(\omega)|^2\, d\omega. \tag{4.15}$$

It is independent of u and ξ. Hence $g_{u,\xi}$ corresponds to a Heisenberg box of area $\sigma_t\, \sigma_\omega$ centered at (u,ξ), as illustrated by Figure 4.2. The size of this box is independent of (u,ξ), which means that a windowed Fourier transform has the same resolution across the time-frequency plane.

Example 4.2. *A sinusoidal wave* $f(t) = \exp(i\xi_0 t)$ *whose Fourier transform is a Dirac* $\hat{f}(\omega) = 2\pi\delta(\omega - \xi_0)$ *has a windowed Fourier transform*

$$Sf(u,\xi) = \hat{g}(\xi - \xi_0)\, \exp[-iu(\xi - \xi_0)]\,.$$

Its energy is spread over the frequency interval $[\xi_0 - \sigma_\omega/2, \xi_0 + \sigma_\omega/2]$.

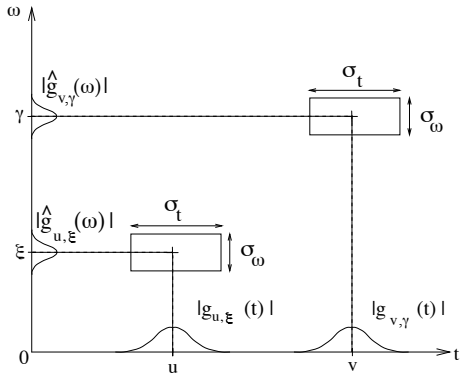

Figure 4.2: Heisenberg boxes of two windowed Fourier atoms $g_{u,\xi}$ and $g_{\nu,\gamma}$.

Example 4.3. *The windowed Fourier transform of a Dirac $f(t) = \delta(t - u_0)$ is*

$$Sf(u,\xi) = g(u_0 - u)\, \exp(-i\xi u_0)\,.$$

Its energy is spread in the time interval $[u_0 - \sigma_t/2, u_0 + \sigma_t/2]$.

Example 4.4. *A linear chirp $f(t) = \exp(iat^2)$ has an "instantaneous frequency" that increases linearly in time. For a Gaussian window $g(t) = (\pi\sigma^2)^{-1/4} \exp[-t^2/(2\sigma^2)]$, the windowed Fourier transform of f is calculated using the Fourier transform (2.34) of Gaussian chirps. One can verify that its spectrogram is*

$$P_S f(u,\xi) = |Sf(u,\xi)|^2 = \left(\frac{4\pi\sigma^2}{1+4a^2\sigma^4}\right)^{1/2} \exp\left(-\frac{\sigma^2(\xi-2au)^2}{1+4a^2\sigma^4}\right). \tag{4.16}$$

For a fixed time u, $P_S f(u,\xi)$ is a Gaussian that reaches its maximum at the frequency $\xi(u) = 2au$. Observe that if we write $f(t) = \exp[i\phi(t)]$, then $\xi(u)$ is equal to the "instantaneous frequency," defined as the derivative of the phase: $\omega(u) = \phi'(u) = 2au$. Section 4.4.1 explains this result.

Example 4.5. *Figure 4.3 gives the spectrogram of a signal that includes a linear chirp, a quadratic chirp and two modulated Gaussians. The spectrogram is computed with a Gaussian window dilated by $\sigma = 0.05$. As expected from (4.16), the linear chirp yields large amplitude coefficients along the trajectory of its instantaneous frequency, which is a straight line. The quadratic chirp yields large coefficients along a parabola. The two modulated Gaussians produce low and high frequency blobs at $u = 0.5$ and $u = 0.87$.*

4.2.1 Completeness and Stability

When the time-frequency indices (u,ξ) vary across $\mathbb{R}^2$, the Heisenberg boxes of the atoms $g_{u,\xi}$ cover the whole time-frequency plane. One can thus expect that f can be recovered from its windowed Fourier transform $Sf(u,\xi)$. The following theorem gives a reconstruction formula and proves that the energy is conserved.

Theorem 4.1. *If $f \in \mathbf{L^2}(\mathbb{R})$ then*

$$f(t) = \frac{1}{2\pi} \int_{-\infty}^{+\infty} \int_{-\infty}^{+\infty} Sf(u,\xi)\, g(t-u)\, \mathrm{e}^{i\xi t}\, d\xi\, du \tag{4.17}$$

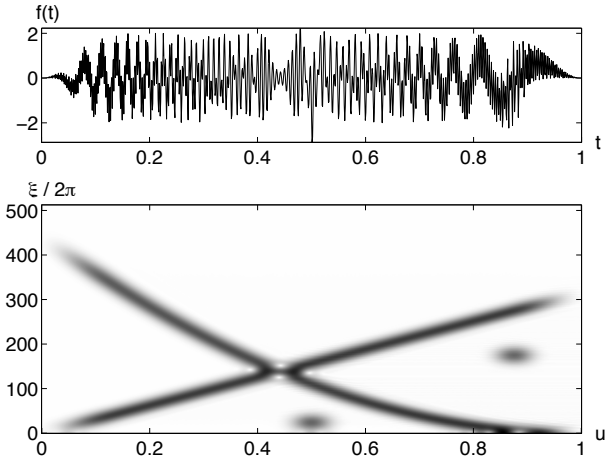

(a)

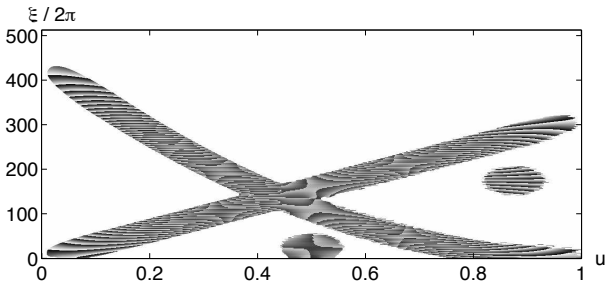

(b)

Figure 4.3: The signal includes a linear chirp whose frequency increases, a quadratic chirp whose frequency decreases, and two modulated Gaussian functions located at $t = 0.5$ and $t = 0.87$. (a) Spectrogram $P_S f(u, \xi)$. Dark points indicate large amplitude coefficients. (b) Complex phase of $Sf(u, \xi)$ in regions where the modulus $P_S f(u, \xi)$ is non-zero.

and

$$\int_{-\infty}^{+\infty} |f(t)|^2\, dt = \frac{1}{2\pi} \int_{-\infty}^{+\infty} \int_{-\infty}^{+\infty} |Sf(u,\xi)|^2\, d\xi\, du. \tag{4.18}$$

Proof. The reconstruction formula (4.17) is proved first. Let us apply the Fourier Parseval formula (2.25) to the integral (4.17) with respect to the integration in u. The Fourier transform of $f_\xi(u) = Sf(u,\xi)$ with respect to u is computed by observing that

$$Sf(u,\xi) = \exp(-iu\xi) \int_{-\infty}^{+\infty} f(t)\, g(t-u)\, \exp[i\xi(u-t)]\, dt = \exp(-iu\xi)\, f \star g_\xi(u),$$

where $g_\xi(t) = g(t)\, \exp(i\xi t)$, because $g(t) = g(-t)$. Its Fourier transform is therefore

$$\hat{f}_\xi(\omega) = \hat{f}(\omega+\xi)\, \hat{g}_\xi(\omega+\xi) = \hat{f}(\omega+\xi)\, \hat{g}(\omega).$$

The Fourier transform of $g(t-u)$ with respect to u is $\hat{g}(\omega)\, \exp(-it\omega)$. Hence

$$\begin{aligned} \frac{1}{2\pi} \left(\int_{-\infty}^{+\infty} \int_{-\infty}^{+\infty} Sf(u,\xi)\, g(t-u)\, \exp(i\xi t)\, du \right) d\xi \quad &= \\ \frac{1}{2\pi} \int_{-\infty}^{+\infty} \left(\frac{1}{2\pi} \int_{-\infty}^{+\infty} \hat{f}(\omega+\xi)\, |\hat{g}(\omega)|^2\, \exp[it(\omega+\xi)]\, d\omega \right) d\xi \quad &. \end{aligned}$$

If $\hat{f} \in \mathbf{L^1}(\mathbb{R})$, we can apply the Fubini Theorem A.2 to reverse the integration order. The inverse Fourier transform proves that

$$\frac{1}{2\pi} \int_{-\infty}^{+\infty} \hat{f}(\omega+\xi)\, \exp[it(\omega+\xi)]\, d\xi = f(t).$$

Since $\frac{1}{2\pi} \int_{-\infty}^{+\infty} |\hat{g}(\omega)|^2\, d\omega = 1$, we derive (4.17). If $\hat{f} \notin \mathbf{L^1}(\mathbb{R})$, a density argument is used to verify this formula.

Let us now prove the energy conservation (4.18). Since the Fourier transform in u of $Sf(u,\xi)$ is $\hat{f}(\omega+\xi)\, \hat{g}(\omega)$, the Plancherel formula (2.26) applied to the right-hand side of (4.18) gives

$$\frac{1}{2\pi} \int_{-\infty}^{+\infty} \int_{-\infty}^{+\infty} |Sf(u,\xi)|^2\, du\, d\xi = \frac{1}{2\pi} \int_{-\infty}^{+\infty} \frac{1}{2\pi} \int_{-\infty}^{+\infty} |\hat{f}(\omega+\xi)\, \hat{g}(\omega)|^2\, d\omega\, d\xi.$$

The Fubini theorem applies and the Plancherel formula proves that

$$\frac{1}{2\pi} \int_{-\infty}^{+\infty} |\hat{f}(\omega+\xi)|^2\, d\xi = \|f\|^2,$$

which implies (4.18). ■ ■

The reconstruction formula (4.17) can be rewritten

$$f(t) = \frac{1}{2\pi} \int_{-\infty}^{+\infty} \int_{-\infty}^{+\infty} \langle f, g_{u,\xi} \rangle\, g_{u,\xi}(t)\, d\xi\, du. \tag{4.19}$$

It resembles the decomposition of a signal in an orthonormal basis but it is not, since the functions $\{g_{u,\xi}\}_{u,\xi \in \mathbb{R}^2}$ are very redundant in $\mathbf{L^2}(\mathbb{R})$. The second equality (4.18) justifies the interpretation of the spectrogram $P_S f(u,\xi) = |Sf(u,\xi)|^2$ as an energy density, since its time-frequency sum equals the signal energy.

Reproducing Kernel A windowed Fourier transform represents a one-dimensional signal $f(t)$ by a two-dimensional function $Sf(u,\xi)$. The energy conservation proves that $Sf \in \mathbf{L^2}(\mathbb{R}^2)$. Because $Sf(u,\xi)$ is redundant, it is not true that any $\Phi \in \mathbf{L^2}(\mathbb{R}^2)$ is the windowed Fourier transform of some $f \in \mathbf{L^2}(\mathbb{R})$. The next theorem gives a necessary and sufficient condition for such a function to be a windowed Fourier transform.

Theorem 4.2. *Let $\Phi \in \mathbf{L^2}(\mathbb{R}^2)$. There exists $f \in \mathbf{L^2}(\mathbb{R})$ such that $\Phi(u,\xi) = Sf(u,\xi)$ if and only if*

$$\Phi(u_0,\xi_0) = \frac{1}{2\pi}\int_{-\infty}^{+\infty}\int_{-\infty}^{+\infty} \Phi(u,\xi)\, K(u_0,u,\xi_0,\xi)\, du\, d\xi, \tag{4.20}$$

with

$$K(u_0,u,\xi_0,\xi) = \langle g_{u,\xi}, g_{u_0,\xi_0}\rangle\ . \tag{4.21}$$

Proof. Suppose that there exists f such that $\Phi(u,\xi) = Sf(u,\xi)$. Let us replace f with its reconstruction integral (4.17) in the windowed Fourier transform definition:

$$Sf(u_0,\xi_0) = \int_{-\infty}^{+\infty}\left(\frac{1}{2\pi}\int_{-\infty}^{+\infty}\int_{-\infty}^{+\infty} Sf(u,\xi)\, g_{u,\xi}(t)\, du\, d\xi\right) g^*_{u_0,\xi_0}(t)\, dt. \tag{4.22}$$

Inverting the integral on t with the integrals on u and ξ yields (4.20). To prove that the condition (4.20) is sufficient, we define f as in the reconstruction formula (4.17):

$$f(t) = \frac{1}{2\pi}\int_{-\infty}^{+\infty}\int_{-\infty}^{+\infty} \Phi(u,\xi)\, g(t-u)\, \exp(i\xi t)\, d\xi\, du$$

and show that (4.20) implies that $\Phi(u,\xi) = Sf(u,\xi)$. ■ ■

Ambiguity Function The reproducing kernel $K(u_0,u,\xi_0,\xi)$ measures the time-frequency overlap of the two atoms $g_{u,\xi}$ and g_{u_0,ξ_0}. The amplitude of $K(u_0,u,\xi_0,\xi)$ decays with u_0-u and $\xi_0-\xi$ at a rate that depends on the energy concentration of g and $\hat{g}$. Replacing $g_{u,\xi}$ and g_{u_0,ξ_0} by their expression and making the change of variable $v = t-(u+u_0)/2$ in the inner product integral (4.21) yields

$$K(u_0,u,\xi_0,\xi) = \exp\left(-\frac{i}{2}(\xi_0-\xi)(u+u_0)\right)\, Ag(u_0-u,\xi_0-\xi) \tag{4.23}$$

where

$$Ag(\tau,\gamma) = \int_{-\infty}^{+\infty} g\left(v+\frac{\tau}{2}\right)\, g\left(v-\frac{\tau}{2}\right)\, \mathrm{e}^{-i\gamma v}\, dv \tag{4.24}$$

is called the *ambiguity function* of g. Using the Parseval formula to replace this time integral with a Fourier integral gives

$$Ag(\tau,\gamma) = \frac{1}{2\pi}\int_{-\infty}^{+\infty} \hat{g}\left(\omega+\frac{\gamma}{2}\right)\, \hat{g}\left(\omega-\frac{\gamma}{2}\right)\, \mathrm{e}^{i\tau\omega}\, d\omega. \tag{4.25}$$

The decay of the ambiguity function measures the spread of g in time and of $\hat{g}$ in frequency. For example, if g has a support included in an interval of size T, then $Ag(\tau,\omega) = 0$ for $|\tau| \geqslant T/2$. The integral (4.25) shows that the same result applies to the support of $\hat{g}$.

4.2.2 Choice of Window

The resolution in time and frequency of the windowed Fourier transform depends on the spread of the window in time and frequency. This can be measured from the decay of the ambiguity function (4.24) or more simply from the area $\sigma_t \, \sigma_\omega$ of the Heisenberg box. The uncertainty Theorem 2.6 proves that this area reaches the minimum value $1/2$ if and only if g is a Gaussian. The ambiguity function $Ag(\tau, \gamma)$ is then a two-dimensional Gaussian.

Window Scale The time-frequency localization of g can be modified with a scaling. Suppose that g has a Heisenberg time and frequency width respectively equal to σ_t and σ_ω. Let $g_s(t) = s^{-1/2} \, g(t/s)$ be its dilation by s. A change of variables in the integrals (4.13) and (4.15) shows that the Heisenberg time and frequency width of g_s are respectively $s\sigma_t$ and σ_ω / s. The area of the Heisenberg box is not modified but it is dilated by s in time and compressed by s in frequency. Similarly, a change of variable in the ambiguity integral (4.24) shows that the ambiguity function is dilated in time and frequency respectively by s and $1/s$

$$Ag_s(\tau, \gamma) = Ag\left(\frac{\tau}{s}, s\gamma\right).$$

The choice of a particular scale s depends on the desired resolution trade-off between time and frequency.

Finite Support In numerical applications, g must have a compact support. Theorem 2.7 proves that its Fourier transform $\hat{g}$ necessarily has an infinite support. It is a symmetric function with a main lobe centered at $\omega = 0$, which decays to zero with oscillations. Figure 4.4 illustrates its behavior. To maximize the frequency resolution of the transform, we must concentrate the energy of $\hat{g}$ near $\omega = 0$. Three important parameters evaluate the spread of $\hat{g}$:

- The root mean-square bandwidth $\Delta\omega$, which is defined by

$$\frac{|\hat{g}(\Delta\omega/2)|^2}{|\hat{g}(0)|^2} = \frac{1}{2}.$$

- The maximum amplitude A of the first side-lobes located at $\omega = \pm\omega_0$ in Figure 4.4. It is measured in decibels:

$$A = 10 \log_{10} \frac{|\hat{g}(\omega_0)|^2}{|\hat{g}(0)|^2}.$$

- The polynomial exponent p, which gives the asymptotic decay of $|\hat{g}(\omega)|$ for large frequencies:

$$|\hat{g}(\omega)| = O(\omega^{-p-1}). \tag{4.26}$$

Table 4.1 gives the values of these three parameters for several windows g whose supports are restricted to $[-1/2, 1/2]$ [292]. Figure 4.5 shows the graph of these windows.

To interpret these three frequency parameters, let us consider the spectrogram of a frequency tone $f(t) = \exp(i\xi_0 t)$. If $\Delta\omega$ is small, then $|Sf(u, \xi)|^2 = |\hat{g}(\xi - \xi_0)|^2$ has an energy concentrated near $\xi = \xi_0$. The side-lobes of $\hat{g}$ create "shadows" at $\xi = \xi_0 \pm \omega_0$, which can be neglected if A is also small.

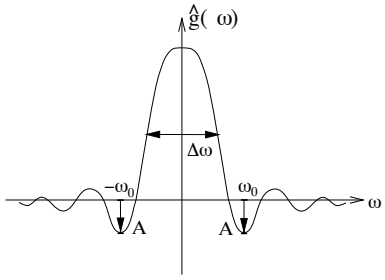

Figure 4.4: The energy spread of $\hat{g}$ is measured by its bandwidth $\Delta\omega$ and the maximum amplitude A of the first side-lobes, located at $\omega = \pm\omega_0$.

Name	$g(t)$	$\Delta\omega$	A	p
Rectangle	1	0.89	-13db	0
Hamming	$0.54 + 0.46\cos(2\pi t)$	1.36	-43db	0
Gaussian	$\exp(-18t^2)$	1.55	-55db	0
Hanning	$\cos^2(\pi t)$	1.44	-32db	2
Blackman	$0.42 + 0.5\cos(2\pi t)$ $+0.08\cos(4\pi t)$	1.68	-58db	2

Table 4.1: Frequency parameters of five windows g whose supports are restricted to $[-1/2, 1/2]$. These windows are normalized so that $g(0) = 1$ but $\|g\| \neq 1$.

If the frequency tone is embedded in a signal that has other components of much higher energy at different frequencies, the tone can still be detected if $\hat{g}(\omega - \xi)$ attenuates these components rapidly when $|\omega - \xi|$ increases. This means that $|\hat{g}(\omega)|$ has a rapid decay, and Theorem 2.5 proves that this decay depends on the regularity of g. Property (4.26) is typically satisfied by windows that are p times differentiable.

4.2.3 Discrete Windowed Fourier Transform

The discretization and fast computation of the windowed Fourier transform follow the same ideas as the discretization of the Fourier transform described in Section 3.3. We consider discrete signals of period N. The window $g[n]$ is chosen to be a symmetric discrete signal of period N with unit norm $\|g\| = 1$. Discrete windowed Fourier atoms are defined by

$$g_{m,l}[n] = g[n-m]\,\exp\left(\frac{i2\pi ln}{N}\right).$$

The discrete Fourier transform of $g_{m,l}$ is

$$\hat{g}_{m,l}[k] = \hat{g}[k-l]\,\exp\left(\frac{-i2\pi m(k-l)}{N}\right).$$

The discrete windowed Fourier transform of a signal f of period N is

$$Sf[m,l] = \langle f, g_{m,l}\rangle = \sum_{n=0}^{N-1} f[n]\,g[n-m]\,\exp\left(\frac{-i2\pi ln}{N}\right), \tag{4.27}$$

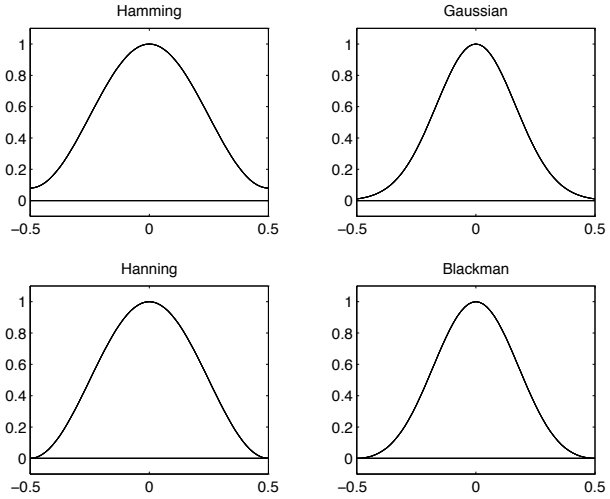

Figure 4.5: Graphs of four windows g whose support are $[-1/2, 1/2]$.

For each $0 \leqslant m < N$, $Sf[m,l]$ is calculated for $0 \leqslant l < N$ with a discrete Fourier transform of $f[n]g[n-m]$. This is performed with N FFT procedures of size N, and thus requires a total of $O(N^2 \log_2 N)$ operations. Figure 4.3 is computed with this algorithm.

Inverse Transform The following theorem discretizes the reconstruction formula and the energy conservation of Theorem 4.1.

Theorem 4.3. *If f is a signal of period N then*

$$f[n] = \frac{1}{N} \sum_{m=0}^{N-1} \sum_{l=0}^{N-1} Sf[m,l]\, g[n-m]\, \exp\left(\frac{i2\pi ln}{N}\right) \tag{4.28}$$

and

$$\sum_{n=0}^{N-1} |f[n]|^2 = \frac{1}{N} \sum_{l=0}^{N-1} \sum_{m=0}^{N-1} |Sf[m,l]|^2. \tag{4.29}$$

This theorem is proved by applying the Parseval and Plancherel formulas of the discrete Fourier transform, exactly as in the proof of Theorem 4.1. The energy conservation (4.29) proves that this windowed Fourier transform defines a tight frame, as explained in Chapter 5. The reconstruction formula (4.28) is rewritten

$$f[n] = \frac{1}{N} \sum_{m=0}^{N-1} g[n-m] \sum_{l=0}^{N-1} Sf[m,l]\, \exp\left(\frac{i2\pi ln}{N}\right).$$

The second sum computes for each $0 \leqslant m < N$ the inverse discrete Fourier transform of $Sf[m,l]$ with respect to l. This is calculated with N FFT procedures, requiring a total of $O(N^2 \log_2 N)$ operations.

A discrete windowed Fourier transform is an N^2 image $Sf[l,m]$ that is very redundant, since it is entirely specified by a signal f of size N. The redundancy is characterized by a discrete reproducing kernel equation, which is the discrete equivalent of (4.20).

4.3 Wavelet Transforms

To analyze signal structures of very different sizes, it is necessary to use time-frequency atoms with different time supports. The wavelet transform decomposes signals over dilated and translated wavelets. A wavelet is a function $\psi \in \mathbf{L^2}(\mathbb{R})$ with a zero average:

$$\int_{-\infty}^{+\infty} \psi(t)\, dt = 0. \tag{4.30}$$

It is normalized $\|\psi\| = 1$, and centered in the neighborhood of $t = 0$. A dictionary of time-frequency atoms is obtained by scaling ψ by s and translating it by u:

$$\mathcal{D} = \left\{ \psi_{u,s}(t) = \frac{1}{\sqrt{s}}\, \psi\left(\frac{t-u}{s}\right) \right\}_{u\in\mathbb{R}, s\in\mathbb{R}^+}.$$

These atoms remain normalized: $\|\psi_{u,s}\| = 1$. The wavelet transform of $f \in \mathbf{L^2}(\mathbb{R})$ at time u and scale s is

$$Wf(u,s) = \langle f, \psi_{u,s}\rangle = \int_{-\infty}^{+\infty} f(t)\, \frac{1}{\sqrt{s}}\, \psi^*\left(\frac{t-u}{s}\right) dt. \tag{4.31}$$

Linear Filtering The wavelet transform can be rewritten as a convolution product:

$$Wf(u,s) = \int_{-\infty}^{+\infty} f(t)\, \frac{1}{\sqrt{s}}\, \psi^*\left(\frac{t-u}{s}\right) dt = f \star \bar{\psi}_s(u) \tag{4.32}$$

with

$$\bar{\psi}_s(t) = \frac{1}{\sqrt{s}}\, \psi^*\left(\frac{-t}{s}\right).$$

The Fourier transform of $\bar{\psi}_s(t)$ is

$$\widehat{\bar{\psi}_s}(\omega) = \sqrt{s}\, \hat{\psi}^*(s\omega). \tag{4.33}$$

Since $\hat{\psi}(0) = \int_{-\infty}^{+\infty} \psi(t)\, dt = 0$, it appears that $\hat{\psi}$ is the transfer function of a band-pass filter. The convolution (4.32) computes the wavelet transform with dilated band-pass filters.

Analytic Versus Real Wavelets Like a windowed Fourier transform, a wavelet transform can measure the time evolution of frequency transients. This requires using a complex analytic wavelet, which can separate amplitude and phase components. The properties of this analytic wavelet transform are described in Section 4.3.2, and its application to the measurement of instantaneous frequencies is explained in Section 4.4.2. In contrast, real wavelets are often used to detect sharp signal transitions. Section 4.3.1 introduces elementary properties of real wavelets, which are developed in Chapter 6.

4.3.1 Real Wavelets

Suppose that ψ is a real wavelet. Since it has a zero average, the wavelet integral

$$Wf(u,s) = \int_{-\infty}^{+\infty} f(t)\, \frac{1}{\sqrt{s}}\, \psi^*\left(\frac{t-u}{s}\right) dt$$

measures the variation of f in a neighborhood of u, whose size is proportional to s. Section 6.1.3 proves that when the scale s goes to zero, the decay of the wavelet coefficients characterizes the regularity of f in the neighborhood of u. This has important applications for detecting transients and analyzing fractals. This section concentrates on the completeness and redundancy properties of real wavelet transforms.

Example 4.6. *Wavelets equal to the second derivative of a Gaussian are called Mexican hats. They were first used in computer vision to detect multiscale edges [487]. The normalized Mexican hat wavelet is*

$$\psi(t) = \frac{2}{\pi^{1/4}\sqrt{3\sigma}} \left(\frac{t^2}{\sigma^2} - 1\right) \exp\left(\frac{-t^2}{2\sigma^2}\right). \tag{4.34}$$

For $\sigma = 1$, Figure 4.6 plots $-\psi$ and its Fourier transform

$$\hat{\psi}(\omega) = \frac{-\sqrt{8}\,\sigma^{5/2}\,\pi^{1/4}}{\sqrt{3}}\,\omega^2\,\exp\left(\frac{-\sigma^2\omega^2}{2}\right). \tag{4.35}$$

Figure 4.7 shows the wavelet transform of a signal that is piecewise regular on the left and almost everywhere singular on the right. The maximum scale is smaller than 1 *because the support of f is normalized to $[0, 1]$. The minimum scale is limited by the sampling interval of the discretized signal used in numerical calculations. When the scale decreases, the wavelet transform has a rapid decay to zero in the regions where the signal is regular. The isolated singularities on the left create cones of large amplitude wavelet coefficients that converge to the locations of the singularities. This is further explained in Chapter 6.*

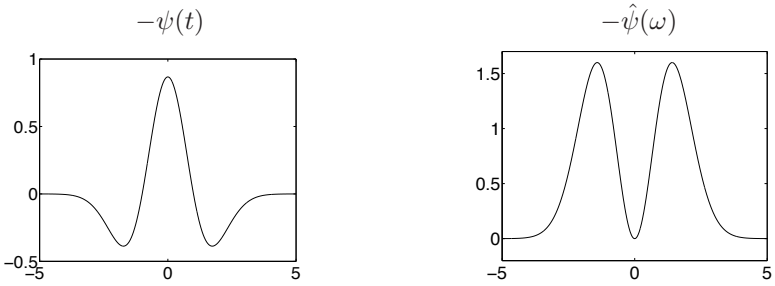

Figure 4.6: Mexican hat wavelet (4.34) for $\sigma = 1$ and its Fourier transform.

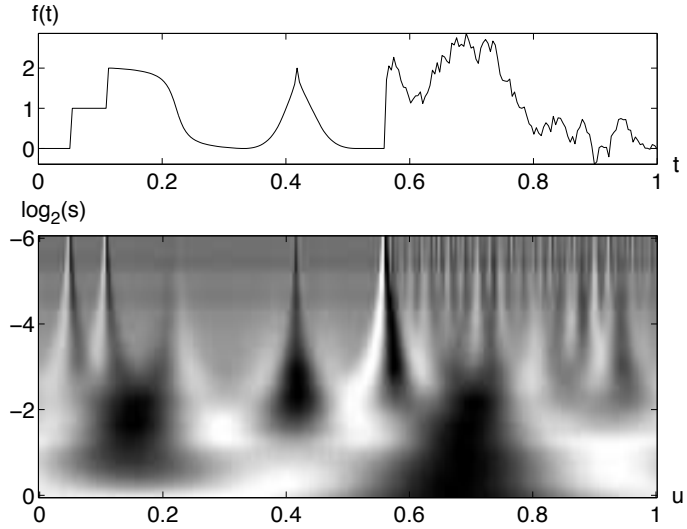

Figure 4.7: Real wavelet transform $Wf(u, s)$ computed with a Mexican hat wavelet (4.34). The vertical axis represents $\log_2 s$. Black, grey and white points correspond respectively to positive, zero and negative wavelet coefficients.

A real wavelet transform is complete and maintains an energy conservation, as long as the wavelet satisfies a weak admissibility condition, specified by the following theorem. This theorem was first proved in 1964 by the mathematician Calderón [131], from a different point of view. Wavelets did not appear as such, but Calderón defines a wavelet transform as a convolution operator that decomposes the identity. Grossmann and Morlet [287] were not aware of Calderón's work when they proved the same formula for signal processing.

Theorem 4.4 (Calderón, Grossmann, Morlet)**.** *Let $\psi \in \mathbf{L^2}(\mathbb{R})$ be a real function such that*

$$C_\psi = \int_0^{+\infty} \frac{|\hat{\psi}(\omega)|^2}{\omega}\, d\omega < +\infty. \tag{4.36}$$

Any $f \in \mathbf{L^2}(\mathbb{R})$ satisfies

$$f(t) = \frac{1}{C_\psi} \int_0^{+\infty} \int_{-\infty}^{+\infty} Wf(u,s)\, \frac{1}{\sqrt{s}}\, \psi\left(\frac{t-u}{s}\right) du\, \frac{ds}{s^2}, \tag{4.37}$$

and

$$\int_{-\infty}^{+\infty} |f(t)|^2 dt = \frac{1}{C_\psi} \int_0^{+\infty} \int_{-\infty}^{+\infty} |Wf(u,s)|^2\, du\, \frac{ds}{s^2}. \tag{4.38}$$

Proof. The proof of (4.38) is almost identical to the proof of (4.18). Let us concentrate on the proof of (4.37). The right integral $b(t)$ of (4.37) can be rewritten as a sum of convolutions. Inserting $Wf(u,s) = f \star \bar{\psi}_s(u)$ with $\psi_s(t) = s^{-1/2}\, \psi(t/s)$ yields

$$\begin{aligned} b(t) &= \frac{1}{C_\psi} \int_0^{+\infty} Wf(.,s) \star \psi_s(t)\, \frac{ds}{s^2} \\ &= \frac{1}{C_\psi} \int_0^{+\infty} f \star \bar{\psi}_s \star \psi_s(t)\, \frac{ds}{s^2}. \end{aligned} \tag{4.39}$$

The "." indicates the variable over which the convolution is calculated. We prove that $b = f$ by showing that their Fourier transforms are equal. The Fourier transform of b is

$$\hat{b}(\omega) = \frac{1}{C_\psi} \int_0^{+\infty} \hat{f}(\omega)\, \sqrt{s}\, \hat{\psi}^*(s\omega)\, \sqrt{s}\, \hat{\psi}(s\omega)\, \frac{ds}{s^2} = \frac{\hat{f}(\omega)}{C_\psi} \int_0^{+\infty} |\hat{\psi}(s\,\omega)|^2\, \frac{ds}{s}.$$

Since ψ is real we know that $|\hat{\psi}(-\omega)|^2 = |\hat{\psi}(\omega)|^2$. The change of variable $\xi = s\omega$ thus proves that

$$\hat{b}(\omega) = \frac{1}{C_\psi} \hat{f}(\omega) \int_0^{+\infty} \frac{|\hat{\psi}(\xi)|^2}{\xi}\, d\xi = \hat{f}(\omega).$$

■ ■

The theorem hypothesis

$$C_\psi = \int_0^{+\infty} \frac{|\hat{\psi}(\omega)|^2}{\omega}\, d\omega < +\infty$$

is called the wavelet *admissibility condition*. To guarantee that this integral is finite we must ensure that $\hat{\psi}(0) = 0$, which explains why we imposed that wavelets must have a zero average. This condition is nearly sufficient. If $\hat{\psi}(0) = 0$ and $\hat{\psi}(\omega)$ is continuously differentiable then the admissibility condition is satisfied. One can verify that $\hat{\psi}(\omega)$ is continuously differentiable if ψ has a sufficient time decay

$$\int_{-\infty}^{+\infty} (1 + |t|)\, |\psi(t)|\, dt < +\infty.$$

Reproducing Kernel Like a windowed Fourier transform, a wavelet transform is a redundant representation, whose redundancy is characterized by a reproducing kernel equation. Inserting the reconstruction formula (4.37) into the definition of the wavelet transform yields

$$Wf(u_0, s_0) = \int_{-\infty}^{+\infty} \left(\frac{1}{C_\psi} \int_0^{+\infty} \int_{-\infty}^{+\infty} Wf(u,s)\, \psi_{u,s}(t)\, du \frac{ds}{s^2} \right) \psi^*_{u_0,s_0}(t)\, dt.$$

Interchanging these integrals gives

$$Wf(u_0, s_0) = \frac{1}{C_\psi} \int_{-\infty}^{+\infty} K(u, u_0, s, s_0)\, Wf(u,s)\, du\, \frac{ds}{s^2}, \tag{4.40}$$

with

$$K(u_0, u, s_0, s) = \langle \psi_{u,s}, \psi_{u_0,s_0} \rangle \ . \tag{4.41}$$

The reproducing kernel $K(u_0, u, s_0, s)$ measures the correlation of two wavelets $\psi_{u,s}$ and ψ_{u_0,s_0}. The reader can verify that any function $\Phi(u,s)$ is the wavelet transform of some $f \in \mathbf{L^2}(\mathbb{R})$ if and only if it satisfies the reproducing kernel equation (4.40).

Scaling Function When $Wf(u,s)$ is known only for $s < s_0$, to recover f we need a complement of information corresponding to $Wf(u,s)$ for $s > s_0$. This is obtained by introducing a *scaling function* ϕ that is an aggregation of wavelets at scales larger than 1. The modulus of its Fourier transform is defined by

$$|\hat{\phi}(\omega)|^2 = \int_1^{+\infty} |\hat{\psi}(s\omega)|^2 \frac{ds}{s} = \int_\omega^{+\infty} \frac{|\hat{\psi}(\xi)|^2}{\xi}\, d\xi, \tag{4.42}$$

and the complex phase of $\hat{\phi}(\omega)$ can be arbitrarily chosen. One can verify that $\|\phi\| = 1$ and we derive from the admissibility condition (4.36) that

$$\lim_{\omega \to 0} |\hat{\phi}(\omega)|^2 = C_\psi. \tag{4.43}$$

The scaling function can thus be interpreted as the impulse response of a low-pass filter. Let us denote

$$\phi_s(t) = \frac{1}{\sqrt{s}}\, \phi\left(\frac{t}{s}\right) \quad \text{and} \quad \bar{\phi}_s(t) = \phi^*_s(-t).$$

The low-frequency approximation of f at the scale s is

$$Lf(u,s) = \left\langle f(t), \frac{1}{\sqrt{s}} \phi\left(\frac{t-u}{s}\right) \right\rangle = f \star \bar{\phi}_s(u). \tag{4.44}$$

With a minor modification of the proof of Theorem 4.4, it can be shown that (Exercise 4.6)

$$f(t) = \frac{1}{C_\psi} \int_0^{s_0} Wf(.,s) \star \psi_s(t)\, \frac{ds}{s^2} + \frac{1}{C_\psi s_0}\, Lf(.,s_0) \star \phi_{s_0}(t). \tag{4.45}$$

Example 4.7. *If ψ is the second order derivative of a Gaussian whose Fourier transform is given by (4.35), then the integration (4.42) yields*

$$\hat{\phi}(\omega) = \frac{2\sigma^{3/2}\pi^{1/4}}{\sqrt{3}} \sqrt{\omega^2 + \frac{1}{\sigma^2}}\, \exp\left(-\frac{\sigma^2\omega^2}{2}\right). \tag{4.46}$$

Figure 4.8 displays ϕ and $\hat{\phi}$ for $\sigma = 1$.

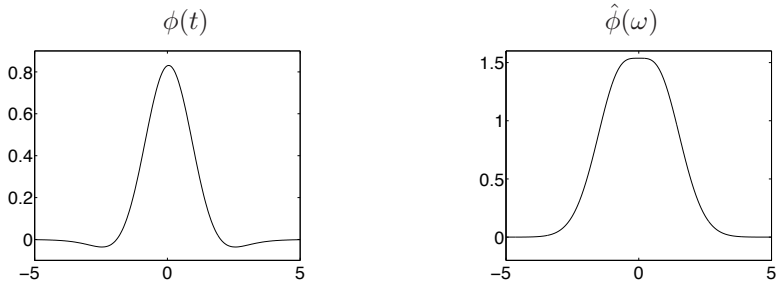

Figure 4.8: Scaling function associated to a Mexican hat wavelet and its Fourier transform calculated with (4.46).

4.3.2 Analytic Wavelets

To analyze the time evolution of frequency tones, it is necessary to use an analytic wavelet to separate the phase and amplitude information of signals. The properties of the resulting analytic wavelet transform are studied.

Analytic Signal A function $f_a \in \mathbf{L^2}(\mathbb{R})$ is said to be *analytic* if its Fourier transform is zero for negative frequencies:

$$\hat{f}_a(\omega) = 0 \quad \text{if } \omega < 0.$$

An analytic function is necessarily complex but is entirely characterized by its real part. Indeed, the Fourier transform of its real part $f = \mathrm{Re}[f_a]$ is

$$\hat{f}(\omega) = \frac{\hat{f}_a(\omega) + \hat{f}_a^*(-\omega)}{2},$$

and this relation can be inverted:

$$\hat{f}_a(\omega) = \begin{cases} 2\,\hat{f}(\omega) & \text{if } \omega \geqslant 0 \\ 0 & \text{if } \omega < 0 \end{cases}. \tag{4.47}$$

The analytic part $f_a(t)$ of a signal $f(t)$ is the inverse Fourier transform of $\hat{f}_a(\omega)$ defined by (4.47).

Discrete Analytic Part The analytic part $f_a[n]$ of a discrete signal $f[n]$ of size N is also computed by setting to zero the negative frequency components of its discrete Fourier transform. The Fourier transform values at $k = 0$ and $k = N/2$ must be carefully adjusted so that $\mathrm{Re}[f_a] = f$ (Exercise 3.22):

$$\hat{f}_a[k] = \begin{cases} \hat{f}[k] & \text{if } k = 0,\ N/2 \\ 2\,\hat{f}[k] & \text{if } 0 < k < N/2 \\ 0 & \text{if } N/2 < k < N \end{cases}. \tag{4.48}$$

We obtain $f_a[n]$ by computing the inverse discrete Fourier transform.

Example 4.8. *The Fourier transform of*

$$f(t) = a\cos(\omega_0 t + \phi) = \frac{a}{2}\Big(\exp[i(\omega_0 t + \phi)] + \exp[-i(\omega_0 t + \phi)]\Big)$$

is

$$\hat{f}(\omega) = \pi a\Big(\exp(i\phi)\,\delta(\omega - \omega_0) + \exp(-i\phi)\,\delta(\omega + \omega_0)\Big).$$

The Fourier transform of the analytic part computed with (4.47) is $\hat{f}_a(\omega) = 2\pi a \exp(i\phi)\,\delta(\omega - \omega_0)$ *and hence*

$$f_a(t) = a \exp[i(\omega_0 t + \phi)]. \tag{4.49}$$

Time-Frequency Resolution An analytic wavelet transform is calculated with an analytic wavelet ψ:

$$Wf(u,s) = \langle f, \psi_{u,s} \rangle = \int_{-\infty}^{+\infty} f(t)\, \frac{1}{\sqrt{s}}\, \psi^*\left(\frac{t-u}{s}\right) dt. \tag{4.50}$$

Its time-frequency resolution depends on the time-frequency spread of the wavelet atoms $\psi_{u,s}$. We suppose that ψ is centered at 0, which implies that $\psi_{u,s}$ is centered at $t = u$. With the change of variable $v = \frac{t-u}{s}$, we verify that

$$\int_{-\infty}^{+\infty} (t-u)^2\, |\psi_{u,s}(t)|^2\, dt = s^2\, \sigma_t^2, \tag{4.51}$$

with $\sigma_t^2 = \int_{-\infty}^{+\infty} t^2\, |\psi(t)|^2\, dt$. Since $\hat{\psi}(\omega)$ is zero at negative frequencies, the center frequency η of $\hat{\psi}$ is

$$\eta = \frac{1}{2\pi} \int_0^{+\infty} \omega\, |\hat{\psi}(\omega)|^2\, d\omega. \tag{4.52}$$

The Fourier transform of $\psi_{u,s}$ is a dilation of $\hat{\psi}$ by $1/s$:

$$\hat{\psi}_{u,s}(\omega) = \sqrt{s}\, \hat{\psi}(s\omega)\, \exp(-i\omega u)\,. \tag{4.53}$$

Its center frequency is therefore η/s. The energy spread of $\hat{\psi}_{u,s}$ around η/s is

$$\frac{1}{2\pi} \int_0^{+\infty} \left(\omega - \frac{\eta}{s}\right)^2 \left|\hat{\psi}_{u,s}(\omega)\right|^2 d\omega = \frac{\sigma_\omega^2}{s^2}, \tag{4.54}$$

with

$$\sigma_\omega^2 = \frac{1}{2\pi} \int_0^{+\infty} (\omega - \eta)^2\, |\hat{\psi}(\omega)|^2\, d\omega.$$

The energy spread of a wavelet time-frequency atom $\psi_{u,s}$ thus corresponds to a Heisenberg box centered at $(u, \eta/s)$, of size $s\sigma_t$ along time and σ_ω/s along frequency. The area of the rectangle remains equal to $\sigma_t\, \sigma_\omega$ at all scales but the resolution in time and frequency depends on s, as illustrated in Figure 4.9.

An analytic wavelet transform defines a local time-frequency energy density $P_W f$, which measures the energy of f in the Heisenberg box of each wavelet $\psi_{u,s}$ centered at $(u, \xi = \eta/s)$:

$$P_W f(u,\xi) = |Wf(u,s)|^2 = \left|Wf\left(u, \frac{\eta}{\xi}\right)\right|^2. \tag{4.55}$$

This energy density is called a *scalogram*.

Completeness An analytic wavelet transform of f depends only on its analytic part f_a. The following theorem derives a reconstruction formula and proves that energy is conserved for real signals.

Theorem 4.5. *For any* $f \in \mathbf{L^2}(\mathbb{R})$

$$Wf(u,s) = \frac{1}{2}\, Wf_a(u,s). \tag{4.56}$$

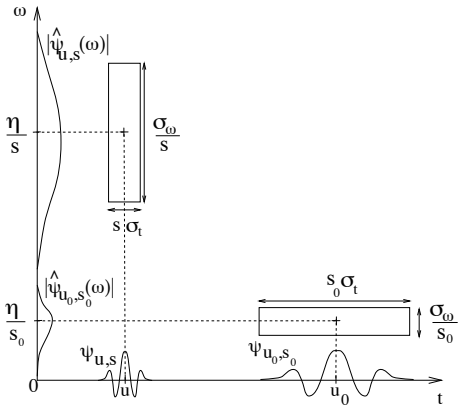

Figure 4.9: Heisenberg boxes of two wavelets. Smaller scales decrease the time spread but increase the frequency support, which is shifted towards higher frequencies.

If $C_\psi = \int_0^{+\infty} \omega^{-1} \, |\hat{\psi}(\omega)|^2 \, d\omega < +\infty$ *and* f *is real then*

$$f(t) = \frac{2}{C_\psi} \mathrm{Re} \left[\int_0^{+\infty} \int_{-\infty}^{+\infty} W f(u,s) \, \psi_s(t-u) \, du \, \frac{ds}{s^2} \right], \tag{4.57}$$

and

$$\|f\|^2 = \frac{2}{C_\psi} \int_0^{+\infty} \int_{-\infty}^{+\infty} |W f(u,s)|^2 \, du \, \frac{ds}{s^2}. \tag{4.58}$$

Proof. Let us first prove (4.56). The Fourier transform with respect to u of

$$f_s(u) = W f(u,s) = f \star \bar{\psi}_s(u)$$

is

$$\hat{f}_s(\omega) = \hat{f}(\omega) \, \sqrt{s} \, \hat{\psi}^*(s\omega).$$

Since $\hat{\psi}(\omega) = 0$ at negative frequencies, and $\hat{f}_a(\omega) = 2\hat{f}(\omega)$ for $\omega \geqslant 0$, we derive that

$$\hat{f}_s(\omega) = \frac{1}{2} \, \hat{f}_a(\omega) \, \sqrt{s} \, \hat{\psi}^*(s\omega),$$

which is the Fourier transform of (4.56).

With the same derivations as in the proof of (4.37) one can verify that the inverse wavelet formula reconstructs the analytic part of f:

$$f_a(t) = \frac{1}{C_\psi} \int_0^{+\infty} \int_{-\infty}^{+\infty} W f_a(u,s) \, \psi_s(t-u) \, \frac{ds}{s^2} \, du. \tag{4.59}$$

Since $f = \mathrm{Re}[f_a]$, inserting (4.56) proves (4.57).

An energy conservation for the analytic part f_a is proved as in (4.38) by applying the Plancherel formula:

$$\int_{-\infty}^{+\infty} |f_a(t)|^2 \, dt = \frac{1}{C_\psi} \int_0^{+\infty} \int_{-\infty}^{+\infty} |W_a f(u,s)|^2 \, du \, \frac{ds}{s^2}.$$

Since $W f_a(u,s) = 2 W f(u,s)$ and $\|f_a\|^2 = 2\|f\|^2$, equation (4.58) follows. ■ ■

If f is real the change of variable $\xi = 1/s$ in the energy conservation (4.58) proves that

$$\|f\|^2 = \frac{2}{C_\psi} \int_0^{+\infty} \int_{-\infty}^{+\infty} P_W f(u,\xi) \, du \, d\xi.$$

It justifies the interpretation of a scalogram as a time-frequency energy density.

Wavelet Modulated Windows An analytic wavelet can be constructed with a frequency modulation of a real and symmetric window g. The Fourier transform of

$$\psi(t) = g(t)\, \exp(i\eta t) \tag{4.60}$$

is $\hat{\psi}(\omega) = \hat{g}(\omega - \eta)$. If $\hat{g}(\omega) = 0$ for $|\omega| > \eta$ then $\hat{\psi}(\omega) = 0$ for $\omega < 0$. Hence ψ is analytic, as shown in Figure 4.10. Since g is real and even, $\hat{g}$ is also real and symmetric. The center frequency of $\hat{\psi}$ is therefore η and

$$|\hat{\psi}(\eta)| = \sup_{\omega \in \mathbb{R}} |\hat{\psi}(\omega)| = \hat{g}(0). \tag{4.61}$$

A *Gabor wavelet* $\psi(t) = g(t)\, \mathrm{e}^{i\eta t}$ is obtained with a Gaussian window

$$g(t) = \frac{1}{(\sigma^2 \pi)^{1/4}}\, \exp\left(\frac{-t^2}{2\sigma^2}\right). \tag{4.62}$$

The Fourier transform of this window is $\hat{g}(\omega) = (4\pi\sigma^2)^{1/4} \exp(-\sigma^2\omega^2/2)$. If $\sigma^2\eta^2 \gg 1$ then $\hat{g}(\omega) \approx 0$ for $|\omega| > \eta$. Such Gabor wavelets are thus considered to be approximately analytic.

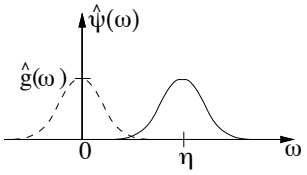

Figure 4.10: Fourier transform $\hat{\psi}(\omega)$ of a wavelet $\psi(t) = g(t)\, \exp(i\eta t)$.

Example 4.9. *The wavelet transform of* $f(t) = a\, \exp(i\omega_0 t)$ *is*

$$W f(u,s) = a\sqrt{s}\, \hat{\psi}^*(s\omega_0)\, \exp(i\omega_0 t) = a\, \sqrt{s}\, \hat{g}(s\omega_0 - \eta)\, \exp(i\omega_0 t).$$

Observe that the normalized scalogram is maximum at $\xi = \omega_0$*:*

$$\frac{\xi}{\eta} P_W f(u,\xi) = \frac{1}{s} |W f(u,s)|^2 = a^2 \left| \hat{g}\left(\eta\Big(\frac{\omega_0}{\xi} - 1\Big)\right)\right|^2.$$

Example 4.10. *The wavelet transform of a linear chirp* $f(t) = \exp(iat^2) = \exp[i\phi(t)]$ *is computed for a Gabor wavelet whose Gaussian window is (4.62). By using the Fourier transform of Gaussian chirps (2.34) one can verify that*

$$\frac{|W f(u,s)|^2}{s} = \left(\frac{4\pi\sigma^2}{1 + 4s^2a^2\sigma^4}\right)^{1/2} \exp\left(\frac{-\sigma^2}{1 + 4a^2s^4\sigma^4}(\eta - 2asu)^2\right).$$

As long as $4a^2s^4\sigma^4 \ll 1$*, at a fixed time* u *the renormalized scalogram* $\eta^{-1}\xi P_W f(u,\xi)$ *is a Gaussian function of* s *that reaches its maximum at*

$$\xi(u) = \frac{\eta}{s(u)} = \phi'(u) = 2\, a\, u. \tag{4.63}$$

Section 4.4.2 explains why the amplitude is maximum at the instantaneous frequency $\phi'(u)$*.*

Example 4.11. *Figure 4.11 displays the normalized scalogram* $\eta^{-1}\xi P_W f(u,\xi)$*, and the complex phase* $\Theta_W(u,\xi)$ *of* $W f(u,s)$*, for the signal* f *of Figure 4.3. The frequency bandwidth of wavelet*

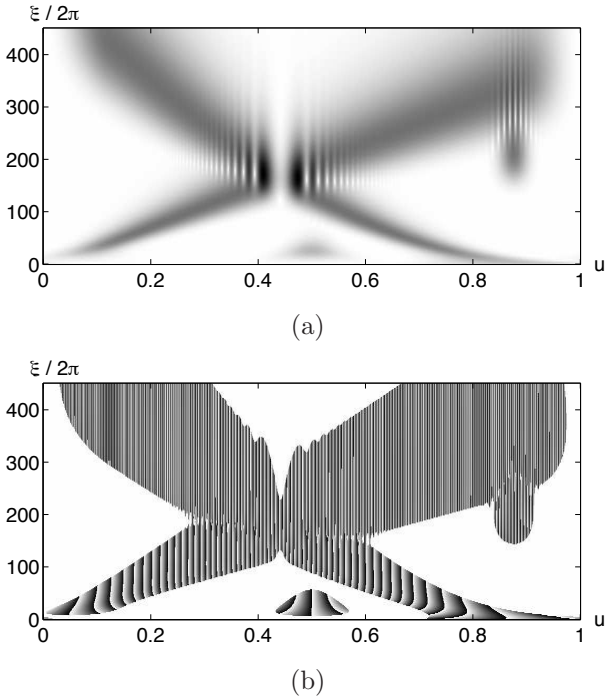

Figure 4.11: (a) Normalized scalogram $\eta^{-1}\xi P_W f(u,\xi)$ computed from the signal in Figure 4.3. Dark points indicate large amplitude coefficients. (b) Complex phase $\Theta_W(u,\xi)$ of $Wf(u,\eta/\xi)$, where the modulus is non-zero.

atoms is proportional to $1/s = \xi/\eta$. *The frequency resolution of the scalogram is therefore finer than the spectrogram at low frequencies but coarser than the spectrogram at higher frequencies. This explains why the wavelet transform produces interference patterns between the high frequency Gabor function at the abscissa* $t = 0.87$ *and the quadratic chirp at the same location, whereas the spectrogram in Figure 4.3 separates them well.*

4.3.3 Discrete Wavelets

Let $\bar{f}(t)$ be a continuous time signal defined over $[0,1]$. Let $f[n]$ be a the discrete signal obtained by a low-pass filtering of $\bar{f}$ and a uniform sampling at intervals N^{-1}. Its discrete wavelet transform can only be calculated at scales $N^{-1} < s < 1$, as shown in Figure 4.7. It is calculated for $s = a^j$, with $a = 2^{1/v}$, which provides v intermediate scales in each octave $[2^j, 2^{j+1})$.

Let $\psi(t)$ be a wavelet whose support is included in $[-K/2, K/2]$. For $1 \leqslant a^j \leqslant N\,K^{-1}$, a discrete wavelet scaled by a^j is defined by

$$\psi_j[n] = \frac{1}{\sqrt{a^j}}\,\psi\left(\frac{n}{a^j}\right).$$

This discrete wavelet has Ka^j non-zero values on $[-N/2, N/2]$. The scale a^j is larger than 1 otherwise the sampling interval may be larger than the wavelet support.

Fast Transform To avoid border problems, we treat $f[n]$ and the wavelets $\psi_j[n]$ as periodic signals of period N. The discrete wavelet transform can then be written as a circular convolution with

$\bar{\psi}_j[n] = \psi_j^*[-n]$:

$$Wf[n, a^j] = \sum_{m=0}^{N-1} f[m]\, \psi_j^*[m-n] = f \circledast \bar{\psi}_j[n]. \tag{4.64}$$

This circular convolution is calculated with the fast Fourier transform algorithm, which requires $O(N \log_2 N)$ operations. If $a = 2^{1/v}$, there are $v \log_2(N/(2K))$ scales $a^j \in [2N^{-1}, K^{-1}]$. The total number of operations to compute the wavelet transform over all scales is therefore $O(vN(\log_2 N)^2)$ [407].

To compute the scalogram $P_W[n, \xi] = |Wf[n, \frac{\eta}{\xi}]|^2$ we calculate $Wf[n, s]$ at any scale s with a parabola interpolation. Let j be the closest integer to $\log_2 s / \log_2 a$, and $p(x)$ be the parabola such that

$$p(j-1) = Wf[n, a^{j-1}] \quad , \quad p(j) = Wf[n, a^j] \quad , \quad p(j+1) = Wf[n, a^{j+1}].$$

A second order interpolation computes

$$Wf[n, s] = p\left(\frac{\log_2 s}{\log_2 a}\right) .$$

Parabolic interpolations are used instead of linear interpolations in order to locate more precisely the ridges defined in Section 4.4.2.

Discrete Scaling Filter A wavelet transform computed up to a scale a^J is not a complete signal representation. It is necessary to add the low frequencies $Lf[n, a^J]$ corresponding to scales larger than a^J. A discrete and periodic scaling filter is computed by sampling the scaling function $\phi(t)$ defined in (4.42):

$$\phi_J[n] = \frac{1}{\sqrt{a^J}}\, \phi\left(\frac{n}{a^J}\right) \quad \text{for } n \in [-N/2, N/2].$$

Let $\bar{\phi}_J[n] = \phi_J^*[-n]$. The low frequencies are carried by

$$Lf[n, a^J] = \sum_{m=0}^{N-1} f[m]\, \phi_J^*[m-n] = f \circledast \bar{\phi}_J[n]. \tag{4.65}$$

Reconstruction An approximate inverse wavelet transform is implemented by discretizing the integral (4.45). Suppose that $a^I = 1$ is the finest scale. Since $ds/s^2 = d\log_e s / s$ and the discrete wavelet transform is computed along an exponential scale sequence $\{a^j\}_j$ with a logarithmic increment $d\log_e s = \log_e a$, we obtain

$$f[n] \approx \frac{\log_e a}{C_\psi} \sum_{j=I}^{J} \frac{1}{a^j}\, Wf[., a^j] \circledast \psi_j[n] + \frac{1}{C_\psi\, a^J}\, Lf[., a^J] \circledast \phi_J[n]. \tag{4.66}$$

The "." indicates the variable over which the convolution is calculated. These circular convolutions are calculated using the FFT, with $O(vN(\log_2 N)^2)$ operations.

Analytic wavelet transforms are often computed over real signals $f[n]$ that have no energy at low frequencies. The scaling filter component is then negligible. Theorem 4.5 shows that

$$f[n] \approx \frac{2 \log_e a}{C_\psi} \operatorname{Re}\left(\sum_{j=I}^{J} \frac{1}{a^j}\, Wf[., a^j] \circledast \psi_j[n] \right) . \tag{4.67}$$

The error introduced by the discretization of scales decreases when the number v of voices per octave increases. However, the approximation of continuous time convolutions with discrete